Axisymmetric Acoustic Scattering by Interpolation

Master's Thesis, Program in Scientific Computing [1]

May 2001

Perrin S. Meyer

Courant Institute of Mathematical Sciences, New York University, NY.

E-mail: meye5148@cims.nyu.edu

We describe and implement a numerical method for the solution of an integral equation arising from the exterior Neumann problem for the Helmholtz equation outside an axisymmetric, doubly connected domain in $\mathbb{R}^3$. The application is the study of acoustic wave propagation through waveguides such as musical horns.

Key Words: Helmholtz, waveguide, axisymmetric, horn

CONTENTS

1. INTRODUCTION

We are interested in the study of how sound propagates through musical horns, for example, a trumpet. In this paper we describe a simple, high-order numerical method for the simulation of sound wave propagation through axisymmetric, sound–hard waveguides. The simplest and widely used musical horns are axisym-

[1] Advisor: Yu Chen. Reader: Leslie Greengard

metric, and the underlying mathematical problem is that of obstacle scattering in $\mathbb{R}^3$, which we will investigate here.

As is well-known, the axisymmetric problem in $\mathbb{R}^3$ can be easily recast as a sequence of obstacle scattering problems in $\mathbb{R}^2$ by means of the rotational symmetry; therefore the efficiency of a computational scheme is not an issue for medium to high frequencies. One of the most efficient mathematical models for the obstacle scattering problem are boundary integral equations based on classical potential theory. With this approach, scattering problems of up to 1000 wavelengths (as measured in the leading linear dimension) can be solved directly with the current hardware; this is more than adequate for most applications in the simulation and design of acoustic horns.

However, the reduction by rotational symmetry makes the resulting Green's function extremely complicated in terms of the algebraic structures of its logarithm singularity, which renders existing spectrally convergent quadrature formulae useless. In fact there is no successful effort, to our best knowledge, in addressing this difficult issue of separating the logarithm singularity from the Green's function to obtain a spectrally convergent quadrature formula for the boundary integral equation.

The solution method we present here avoids the separation of the singularity, and at the same time maintains spectral convergence, all at the expense of a higher condition number of the resulting linear system to be solved. The high condition number does not cause any instability (see Section 8) but the spectral convergence stops when the error drops to about 10^{-8}.

A major advantage of the new approach is the simplicity of coding. There is no need to design quadratures for singular integrals and only discrete points are needed on the curves and surfaces of the scatterer, not "elements", or collections of low–order spline curves or surfaces.

2. ACOUSTIC BACKGROUND

If sound waves propagating in air are low intensity, the acoustic propagation of these waves is well modeled by a linearization of the Euler equations of gas dynamics [19] which results in the linear wave equation

$$\nabla^2 p(\mathbf{x}, t) - \frac{1}{c^2} \frac{\partial^2 p(\mathbf{x}, t)}{\partial t^2} = 0 \tag{1}$$

where $\mathbf{x}$ is a point in $\mathbb{R}^3$, $p(\mathbf{x}, t)$ is an acoustic pressure disturbance field, t is time, and c is the speed of sound[2]. Air does not become appreciably non–linear until well above the levels required to produce immediate hearing damage in humans, and so this linearization is valid for sounds created by musical instruments, or even from sound produced by high–power loudspeakers. c varies with changes in atmospheric pressure, temperature, and humidity, but for small acoustic problems it can assumed to be constant. Here by "small" we mean sound propagation in still air with distances of less than a hundred meters. The value commonly used for room temperature and standard atmospheric pressure is a wave speed of 343 meters per second.

[2]In our notation we will use bold to denote variables that represent points in $\mathbb{R}^3$

Under the standard time-harmonic assumption, and with ω as the angular frequency

$$p(\mathbf{x}, t) = \text{Real}\{u(\mathbf{x})e^{-i\omega t}\} \tag{2}$$

we find that u satisfies the Helmholtz equation

$$\triangle u(\mathbf{x}) + k^2\, u(\mathbf{x}) = 0 \tag{3}$$

where k is the wavenumber $k = \frac{\omega}{c}$, and $\nabla^2 = \triangle$.

3. STATEMENT OF PROBLEM

We wish to solve an exterior Neumann axisymmetric scattering problem. Given a continuous function g on ∂D, find a radiating solution $u \in C^2(\mathbb{R}^3 \setminus \bar{D}) \cap C(\mathbb{R}^3 \setminus D)$ to the Helmholtz equation

$$\triangle u + k^2 u = 0 \quad \text{in } \mathbb{R}^3 \setminus \bar{D} \tag{4}$$

which satisfies the boundary condition

$$\frac{\partial u}{\partial \nu} = g \quad \text{on } \partial D \tag{5}$$

in the sense of uniform convergence on ∂D. Let D be a doubly connected domain in $\mathbb{R}^3$. We assume the boundary ∂D to be connected and of class $C^{2,\beta}$. by ν we denote the unit normal vector to the boundary ∂D directed to the exterior of D.

4. AXISYMMETRIC FORMULATION

We are interested in modeling sound waves propagation through an axisymmetric waveguides in $\mathbb{R}^3$. As is well-known, at high frequencies or large k, the computational requirements for the Helmholtz equation are very large. Methods for solving the Helmholtz equation based on numerically solving boundary integral equations produce large, dense, and complex systems of linear equations that need to be solved, and the linear system is different for every wave number k. Direct methods for even medium size k can produce dense matrices on the order of 30,000 by 30,000, requiring tens of Gigabytes of main memory storage, and hundreds of hours of computer time [5]. Even if iterative methods are used [20], the storage and computational costs are enormous. Efficient numerical methods are still an active research topic [4, 9, 23, 24, 6, 22, 14]. The Fast Multipole Method (FMM) can reduce the storage costs from n^2 (where n is the number of points or elements used to discretize the scatterer) to $\mathrm{O}(n \log_2 n)$ and the computational costs to $\mathrm{O}(n \log^2 n)$. Unfortunately, a multilevel adaptive FMM for the Helmholtz equation is extremely difficult to code, and to our knowledge, there are no free or open–source implementations currently available.

However, an axisymmetric obstacle scattering problem in $\mathbb{R}^3$, which we will investigate, can easily be reduced to a sequence of obstacle scattering problems in $\mathbb{R}^2$; therefore the issue of efficiency is minimal. In fact, such a scattering problem can be solved up to size 1000 wavelengths on current workstations.

The following equations describe our axisymmetric formulation. Let $\hat{x}, \hat{y}, \hat{z}$ denote the Cartesian coordinate system. If $x(t)$ is the $\hat{x}$ component of a simple curve

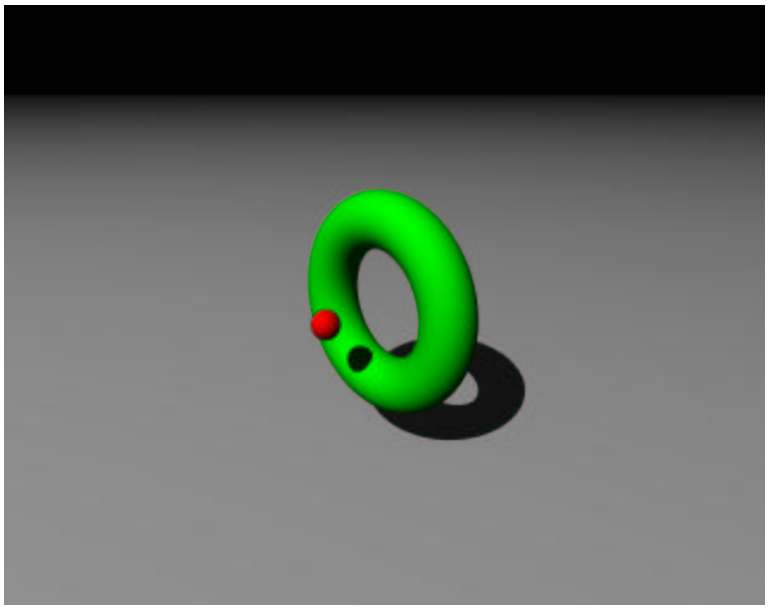

FIG. 1. This figure shows a rendering of a green torus. The red sphere shows the location of the point source creating an incident sound field.

parameterized by t, and $y(t)$ is the $\hat{y}$ component of the same curve parameterized by t, then if we rotate this curve around the $\hat{x}$ axis, the equation for the scattering surface $\mathbf{y}(t,\theta)$ (denoted by ∂D, and parameterized by t and θ) described by this rotation is

$$\mathbf{y}(t,\theta) = x(t)\hat{x} + y(t)\cos(\theta)\hat{y} + y(t)\sin(\theta)\hat{z} \tag{6}$$

For example, if $x(t) = 3+\cos(t)$ and $y(t) = 3+\sin(t)$, $0 \leq t \leq 2\pi$, the surface–of–rotation ∂D is the green torus shown in figure 1. The red sphere shows the location of a point source that creates the incident scattering field.

5. SOLUTIONS BASED ON SINGLE AND DOUBLE LAYER POTENTIAL THEORY

Because we are interested in homogeneous free–space scattering, it is natural to recast the Helmholtz equation into a boundary integral formulation on the surface of the scatterer ∂D.

Colton and Kress [10] describe a solution of the exterior Neumann Helmholtz equation by using a combined single and double layer approach from potential theory.

We seek solutions in the form

$$u(\mathbf{x}) = \int_{\partial D} \left(\Phi(\mathbf{x},\mathbf{y})\varphi(\mathbf{y}) + i\eta \frac{\partial \Phi(\mathbf{x},\mathbf{y})}{\partial \nu(\mathbf{y})} \varphi(\mathbf{y}) \right) ds(\mathbf{y}), \quad \mathbf{x} \notin \partial D \tag{7}$$

with continuous density φ and a real coupling parameter $\eta \neq 0$. Equation (7) solves the exterior Neumann problem provided the density is a solution to the second–kind integral equation

$$\varphi - K'\varphi - i\eta T\varphi = -2g \tag{8}$$

where the integral operators K' and T are

$$(K'\varphi)(\mathbf{x}) = 2\int_{\partial D} \frac{\partial \Phi(\mathbf{x},\mathbf{y})}{\partial \nu(\mathbf{x})}\varphi(\mathbf{y})\, ds(\mathbf{y}) \quad \mathbf{x} \in \partial D \tag{9}$$

$$(T\varphi)(\mathbf{x}) = 2\frac{\partial}{\partial \nu(\mathbf{x})}\int_{\partial D} \frac{\partial \Phi(\mathbf{x},\mathbf{y})}{\partial \nu(\mathbf{y})}\varphi(\mathbf{y}) ds(\mathbf{y}), \quad \mathbf{x} \in \partial D \tag{10}$$

This solution is unique for all (positive) wavenumbers k. If the coupling parameter is chosen to be $\eta = 0$, then the single layer formulation is non-unique when k^2 is an interior Dirichlet eigenvalue of $-\triangle$, often known as an "internal resonance."

We note that technical difficulties arise when implementing a numerical method based on equation (8) because of the hypersingular operator T. Kress [16] describes a method attributed to Maue that can be used to overcome this difficulty.

Grannel et. al. [13] describe a method first proposed in the acoustics literature by Burton that uses a combination of only weakly singular integral operators. K' and T are as defined above, and

$$(V\varphi)(\mathbf{x}) = \int_{\Gamma} \Phi(\mathbf{x},\mathbf{y})\varphi(\mathbf{y}) ds(\mathbf{y}), \quad \mathbf{x} \in \partial D \tag{11}$$

$$(K\varphi)(\mathbf{x}) = \int_{\Gamma} \frac{\partial \Phi(\mathbf{x},\mathbf{y})}{\partial \nu(\mathbf{y})}\varphi(\mathbf{y})\, ds(\mathbf{y}), \quad \mathbf{x} \in \partial D \tag{12}$$

The integral equation suggested is

$$[I + K + \alpha V_0(T - T_0) + \alpha(K_0^2 - I)]u = [V + \alpha V_0(K' - I)]g \tag{13}$$

where the zero subscript on an operator signifies that operator in the "static" limit $k = 0$.

6. NUMERICAL SOLUTION OF THE EXTERIOR NEUMANN PROBLEM IN $\mathbb{R}^2$

Kress [16] describes a numerical method for the solution of the exterior Neumann problem in $\mathbb{R}^2$ (cylindrical scattering). It solves the second–kind integral equation (8) using a Nyström method on analytic boundary curves described by trigonometric interpolating polynomials. By properly treating the logarithmic singularity in the fundamental solution of the Helmholtz equation in $\mathbb{R}^2$, the method achieves superalgebraic convergence for analytic boundary curves.

We had originally hoped to modify this method for the solution of our axisymmetric scattering problem, because by assuming axisymmetric symmetry, we are in effect reducing our scattering problem in $\mathbb{R}^3$ to a one dimensional boundary integral in $\mathbb{R}^2$. The axisymmetric kernel has a logarithmic singularity, but we found it impossible to find a suitable splitting of the axisymmetric kernel in the form $\ln(kR(\mathbf{x},\mathbf{y}))K_1(\mathbf{x},\mathbf{y}) + K_2(\mathbf{x},\mathbf{y})$ in order to use the Nyström method. We sketch the method because of its elegance and in the hope that someone will direct us to a suitable splitting that would allow us to use this method on our axisymmetric scattering problem.

In two dimensions, the fundamental solution to the Helmholtz equation is

$$\Phi(x,y) := \frac{i}{4}H_0^{(1)}(\kappa|x-y|), \quad x \neq y \tag{14}$$

where H_n is a *Hankel* function of the first kind of order n (see [10, 1]).

$$H_n^{(1,2)} := J_n \pm iY_n \tag{15}$$

where J_n are *Bessel* functions of order n

$$J_n(t) := \sum_{p=0}^{\infty} \frac{(-1)^p}{p!(n+p)!} \left(\frac{t}{2}\right)^{n+2p} \tag{16}$$

and Y_n are *Neumann* functions of order n

$$\begin{aligned} Y_n(t) := \frac{2}{\pi}\{\ln\frac{t}{2} + C\}J_n(t) - \frac{1}{\pi}\sum_{p=0}^{n-1}\frac{(n-1-p)!}{p!}\left(\frac{2}{t}\right)^{n-2p} \\ - \frac{1}{\pi}\sum_{p=0}^{\infty}\frac{(-1)^p}{p!(n+p)!}\left(\frac{t}{2}\right)^{n+2p}\{\psi(p+n)+\psi(p)\} \end{aligned} \tag{17}$$

Kress assumes the that the boundary curve ∂D possesses a regular analytic and 2π periodic parametric representation of the form

$$x(t) = (x_1(t), x_2(t)), \quad 0 \le t \le 2\pi \tag{18}$$

in a counterclockwise orientation satisfying $[x_1'(t)]^2 + [x_2'(t)]^2 > 0$ for all t. By straightforward calculations using $H_1^{(1)} = -H_0^{(1)'}$, we transform the single layer integral equation into the parametric form.

$$\psi(t) - \frac{i}{2}\int_0^{2\pi} \frac{\partial H_0^{(1)}(\kappa\, r)}{\nu(t)}\psi(\tau)\, ds(\tau) = -2g_0(t) \tag{19}$$

where

$$r(t,\tau) := \{[x_1(t) - x_1(\tau)]^2 + [x_2(t) - x_2(\tau)]^2\}^{\frac{1}{2}} \tag{20}$$

After some algebra, we can reduce this equation to the form

$$\psi(t) - \int_0^{2\pi} K(t,\tau)\,\psi(\tau)d\tau = g(t), \quad 0 \le t \le 2\pi \tag{21}$$

$$\begin{aligned} K(t,\tau) = \frac{i\,\kappa\, H_1^{(1)}(\kappa\, r(t,\tau))}{2\, r(t,\tau)}\{x_2'(t)[x_1(\tau) - x_1(t)] - x_1'(t)[x_2(\tau) - x_2(t)]\} \\ \frac{\{[x_1'(\tau)]^2 + [x_2'(\tau)]^2\}^{\frac{1}{2}}}{\{[x_1'(t)]^2 + [x_2'(t)]^2\}^{\frac{1}{2}}} \end{aligned} \tag{22}$$

If we split the kernel K into two parts

$$K(t,\tau) = K_1(t,\tau)\ln\left(4\sin^2\frac{t-\tau}{2}\right) + K_2(t,\tau) \tag{23}$$

$$K_1(t,\tau) = \frac{-k}{2\pi}\frac{J_1(k\,r(t,\tau))}{r(t,\tau)}\{x_2'(t)[x_1(\tau)-x_1(t)] - x_1'(t)[x_2(\tau)-x_2(t)]\} \frac{\{[x_1'(\tau)]^2+[x_2'(\tau)]^2\}^{\frac{1}{2}}}{\{[x_1'(t)]^2+[x_2'(t)]^2\}^{\frac{1}{2}}} \quad (24)$$

$$K_2(t,\tau) = K(t,\tau) - K_1(t,\tau)\ln\left(4\sin^2\frac{t-\tau}{2}\right) \quad (25)$$

K_1 and K_2 are analytic, and the diagonal terms are

$$K_2(t,t) = K(t,t) = \frac{1}{2\pi}\frac{x_2'(t)x_1''(t) - x_1'(t)x_2''(t)}{[x_1'(t)]^2+[x_2'(t)]^2} \quad (26)$$

(and $K_1 = 0$). The Nyström method consists in the straightforward approximation of the integrals by quadrature formulas. For the 2π periodic integrands, we choose an equidistant set of knots

$$t_j := \frac{\pi j}{n}, \quad j = 0,\ldots,2n-1, \quad (27)$$

and the quadrature rule

$$\int_0^{2\pi} \ln\left(4\sin^2\frac{t-\tau}{2}\right) f(\tau)d\tau \approx \sum_{j=0}^{2n-1} R_j^{(n)}(t) f(t_j), \quad 0 \le t \le 2\pi \quad (28)$$

with the quadrature weights given by

$$R_j^{(n)}(t) := -\frac{2\pi}{n}\sum_{m=1}^{n-1}\frac{1}{m}\cos m(t-t_j) - \frac{\pi}{n^2}\cos n(t-t_j), \quad j = 0,\ldots,2n-1,$$

and the trapezoidal rule

$$\int_0^{2\pi} f(\tau)d\tau \approx \frac{\pi}{n}\sum_{j=0}^{2n-1} f(t_j) \quad (29)$$

Both these numerical integration formulas are obtained by replacing the integrand f by its trigonometric interpolation polynomial and then integrating exactly. In the Nyström method, the integral equation is replaced by the approximating equation

$$\psi^{(n)}(t) - \sum_{j=0}^{2n-1}\{R_j^{(n)}(t)K_1(t,t_j) + \frac{\pi}{n}K_2(t,t_j)\}\psi^{(n)}(t_j) = g(t) \quad (30)$$

(3.72) reduces to solving a linear system of equations

$$\psi_i^{(n)} - \sum_{j=0}^{2n-1}\{R_{|i-j|}^{(n)}K_1(t_i,t_j) + \frac{\pi}{n}K_2(t_i,t_j)\}\psi_j^{(n)} = g(t_i) \quad (31)$$

for $i = 0,1,\ldots,2n-1$, where

$$R_j^{(n)} := R_j^{(n)}(0) = -\frac{2\pi}{n}\sum_{m=1}^{n-1}\frac{1}{m}\cos\frac{mj\pi}{n} - \frac{(-1)^j\pi}{n^2}, \quad j = 0,\ldots,2n-1, \quad (32)$$

7. SINGULARITIES IN THE AXISYMMETRIC KERNEL

In order to solve the three dimensional axisymmetric scattering problem, we need an an expression for the axisymmetric free space Green's function. $\mathbf{x}$ and $\mathbf{y}$ are points in $\mathbb{R}^3$ on the surface of rotation ∂D. In order to keep the notation similar to the discussion of the Nyström method in $\mathbb{R}^2$, we will again parameterize our two dimensional boundary curve with trigonometric interpolating polynomials x and y indexed by t and τ, but with the additional variables θ_t and θ_τ which describe angle of the surface of rotation. $\mathbf{x}$ and $\mathbf{y}$ are then defined as

$$\mathbf{x}(t,\theta_t) = x(t)\hat{x} + y(t)\cos(\theta_t)\hat{y} + y(t)\sin(\theta_t)\hat{z} \tag{33}$$

$$\mathbf{y}(\tau,\theta_\tau) = x(\tau)\hat{x} + y(\tau)\cos(\theta_\tau)\hat{y} + y(\tau)\sin(\theta_\tau)\hat{z} \tag{34}$$

If we define $R(\mathbf{x},\mathbf{y})$ as the distance between points $\mathbf{x}$ and $\mathbf{y}$,

$$R(\mathbf{x},\mathbf{y}) = \sqrt{[x(t)-x(\tau)]^2 + [y(t)\cos(\theta_t) - y(\tau)\cos(\theta_\tau)]^2 + [y(t)\sin(\theta_t) - y(\tau)\sin(\theta_\tau)]^2} \tag{35}$$

For simplicity in notation, and to be consistent with [13, 18], we introduce the functions $a(t,\tau)$ and $b(t,\tau)$, and from simple trigonometric reduction derive an expression for $R(\mathbf{x},\mathbf{y})$ for $\mathbf{x}$ and $\mathbf{y}$ on ∂D

$$a(t,\tau) = (x(t)-x(\tau))^2 + y^2(t) + y^2(\tau) \tag{36}$$

$$b(t,\tau) = 2\,y(t)\,y(\tau) \tag{37}$$

$$R(t,\tau,\theta_t,\theta_\tau) = (a(t,\tau) - b(t,\tau)\,\cos(\theta_t - \theta_\tau))^{\frac{1}{2}} \tag{38}$$

If we assume that our boundary conditions are also axisymmetric $g(t,\theta_t) = g(t,0)$, then for our axisymmetric horn the surface integral operators are effectively replaced with one-dimensional integral operators over ∂D. Recall that the free space Green's function for the Helmholtz equation in $\mathbb{R}^3$ is

$$\Phi(\mathbf{x},\mathbf{y}) = \frac{1}{4\pi}\frac{e^{ikR}}{R} \tag{39}$$

Because R now only depends on $R(t,\tau,\theta)$, we obtain axisymmetric kernels of the form

$$\mathbf{K}(t,\tau) = \frac{1}{4\pi}\int_0^{2\pi} \frac{e^{i\,k\,R}}{R} d\theta \tag{40}$$

When $t = \tau$ and $\theta = 0$, the kernel in equation (40) becomes singular, and in order to solve the boundary integral equation numerically the singularity must be dealt with.

For our first attempt at treating the singularity in the axisymmetric kernel, we followed a suggestion from [13]. They described a method where they subtract out the $\int \frac{1}{R}$ logarithmic singularity (which is static, i.e. not dependent on k):

$$\int_o^{2\pi} \frac{e^{ikR}}{R} = \int_o^{2\pi} \frac{e^{ikR}-1}{R} + \int_o^{2\pi} \frac{1}{R} \tag{41}$$

After suitable manipulation, this equation can be recast as a hypergeometric series. From [1, 13, 12, 17], $\int_0^{2\pi} \frac{1}{R}\, d\,\theta_\tau$ is a complete elliptic integral of the first kind $K_e(m)$ which can be written as a hypergeometric series $H(\alpha, \beta; c; z)$

$$\int_0^{2\pi} \frac{1}{R(t,\tau,\theta_\tau)}\, d\,\theta_\tau = 2\, g(t,\tau)\, K_e(m(t,\tau)) = g(t,\tau)\, \pi\, H(\frac{1}{2}, \frac{1}{2}; 1; m(t,\tau)) \tag{42}$$

$$m(t,\tau) = \frac{2\, b(t,\tau)}{a(t,\tau) + b(t,\tau)}, \quad g(t,\tau) = \frac{2}{\sqrt{a(t,\tau) + b(t,\tau)}} \tag{43}$$

$$K_e(m) = \frac{1}{2}\, \pi\, H(\frac{1}{2}, \frac{1}{2}; 1; m) \tag{44}$$

$$H(\alpha, \beta; \alpha + \beta; m) = \tag{45}$$

$$\frac{\Gamma(\alpha+\beta)}{\Gamma(\alpha)\,\Gamma(\beta)} \sum_{n=0}^{\infty} \frac{(\alpha)_n\, (\beta)_n}{(n!)^2} [2\psi(n+1) - \psi(\alpha+n) - \psi(\beta+n) - \ln(1-m)](1-m)^n \tag{46}$$

$$\int_0^{2\pi} \frac{1}{R(t,\tau,\theta_\tau)} = \int_0^{2\pi} \frac{d\theta}{\sqrt{a(t,\tau) - b(t,\tau)\, \cos(\theta)}} = \tag{47}$$

$$= \frac{2}{\pi\, \sqrt{a+b}} \sum_{n=0}^{\infty} \left(\frac{\Gamma\left(\frac{1}{2}+n\right)}{(n!)} \right)^2 \left(\frac{a-b}{a+b} \right)^n \left(2\Psi(n+1) - 2\Psi\left(\frac{1}{2}+n\right) - \ln\left(\frac{a-b}{a+b}\right) \right) \tag{48}$$

$$\Gamma(z) = \int_0^{\infty} t^{z-1}\, e^{-t} dt \quad \text{Gamma Function} \tag{49}$$

$$\psi(z) = \frac{d[\ln(\Gamma(z))]}{dz} \quad \text{Psi (Digamma) Function} \tag{50}$$

From these equations, we can write an explicit expression for the logarithmic singularity

$$\ln(a(t,\tau) - b(t,\tau)) \underbrace{\left(\frac{2L(t)}{\pi\, \sqrt{a(t,\tau) + b(t,\tau)}} \right) \sum_{n=0}^{\infty} \left(\frac{\Gamma(n+\frac{1}{2})}{n!} \right)^2 \left(\frac{a(t,\tau) - b(t,\tau)}{a(t,\tau) + b(t,\tau)} \right)^n}_{K_1(t,\tau)} \tag{51}$$

Unfortunately, this singularity extraction does not completely treat the logarithmic singularity, as noted [5, 4], because the derivatives of $\frac{e^{ikR}-1}{R}$ are unbounded. This would limit the convergence of the previously described Nyström method to a low order method.

Kress directed us to paper he had written about the magnetic confinement of an electrically conducting fluid in a torus (with applications in fusion research)[15], which happens to have the same form as our exterior Neumann axisymmetric scattering problem. In this paper, he includes a more involved procedure in order to treat the logarithmic singularity: "For a satisfactory numerical approximation a careful investigation of the nature of the singularity of the kernels is necessary. Since essentially we are solving a two-dimensional boundary–value problem in the

cross–section of ∂D we expect a logarithmic singularity when $t = \tau$." Here, he defines (for integers m) the integrals

$$I_m(t,\tau) = \int_0^{2\pi} [R(t,\tau,\theta)]^{m-1} d\theta \tag{52}$$

and

$$J_m(t,\tau) = \int_0^{2\pi} \cos(\theta)[R(t,\tau,\theta)]^{m-1} d\theta \tag{53}$$

where $R(t,\tau,\theta)$ are as defined in (38) (with $\theta_\tau = 0$). Through partial integration, Kress introduces the recurrence equations

$$I_{m+2} = pI_m - qJ_m \tag{54}$$

and

$$(m+3)J_{m+2} = (m+1)[pJ_m - qI_m] \tag{55}$$

where for even indices the initial terms are given through

$$I_0 = \frac{4}{(p+q)^{\frac{1}{2}}} K(\hat{k}) \tag{56}$$

and

$$J_0 = \frac{4}{q(p+q)^{\frac{1}{2}}} [pK(\hat{k}) - (p+q)E(\hat{k})] \tag{57}$$

where

$$p(t,\tau) = [y(t)]^2 + [y(\tau)]^2 + [x(t) - x(\tau)]^2$$

and

$$q(t,\tau) = 2y(t)y(\tau)$$

where

$$\hat{k}(t,\tau) = \left(\frac{2q(t,\tau)}{p(t,\tau) + q(t,\tau)} \right)^{\frac{1}{2}}$$

and E and K denote the complete elliptic integrals

$$E(\hat{k}) = \int_0^{2\pi} (1 - \hat{k}^2 \sin^2(\theta))^{\frac{1}{2}} d\theta$$

$$K(\hat{k}) = \int_0^{2\pi} (1 - \hat{k}^2 \sin^2(\theta))^{-\frac{1}{2}} d\theta$$

After a few more pages of manipulation of this sorts he arrives at a suitable splitting of the axisymmetric kernels in the form $\ln(K_s(t,\tau))K_1(t,\tau) + K_2(t,\tau)$, where for analytic boundary cross sections of the torus the kernels K_1 and K_2 are analytic. He then uses the exact same Nyström quadrature method with trigonometric interpolation polynomials as described above for the $\mathbb{R}^2$ case to solve the boundary integral equations in this axisymmetric setting.

Unfortunately, as he states on page 337: "Note that equations (54) and (55) are unstable, but they can be transformed into recurrence relations for $\hat{I}_m = \frac{k^m}{m!} I_m$ and $\hat{J}_m = \frac{k^m}{m!} J_m$ which turn out to be stable for k not too large." Also unfortunately, he gives no estimate of what "too large" is.

We found in our own numerical tests that this recursion scheme is unstable (in double precision) for ka greater than approximately 5, where a is a characteristic length scale (1 in our tests). This would limit the usefulness of this scheme as a numerical method to only low frequency scattering problems, despite the high–order convergence.

8. OBSTACLE SCATTERING BY INTERPOLATION

Because of the difficulties in finding a suitable splitting of the logarithmic singularity in the axisymmetric formulation, we decided to develop a numerical solution method based on solving a first–kind integral equation by interpolation. In this formulation, the points $\mathbf{x}$ and $\mathbf{y}$ never coincide, and the kernels are thus never singular. The following method is based on a seminar given on 9 October 2000 at the Courant Institute, presented by Yu Chen.[8]

We note that many others have solved Helmholtz scattering problems by solving a first–kind integral equation. In the literature, this has been called a "Null Field" or "T–matrix" method, for example. A recent review summarizes these methods under the name "discrete source" methods [11].

Our method is described below.

We assume that the obstacle D is surrounded by a homogeneous medium, referred to as the free space.

We will adopt the point of view that a wave, incident or scattered, is generated by its sources: (i) The incident wave u_0 by sources outside D (ii) The scattered wave v by sources on the scattering surface ∂D.

For simplicity, we assume that the incident wave is generated by a point source at $\mathbf{x}_0$ outside D,

$$u_0(\mathbf{x}) = \frac{1}{4\pi} \frac{e^{ik|\mathbf{x}-\mathbf{x}_0|}}{|\mathbf{x}-\mathbf{x}_0|} \quad \mathbf{x} \neq \mathbf{x}_0 \tag{58}$$

Outside the support of its sources, a time–harmonic wave w in free space satisfies the Helmholtz equation

$$\triangle w(\mathbf{x}) + k^2 w(\mathbf{x}) = 0 \tag{59}$$

where $k = \frac{\omega}{c}$ is the wavenumber, ω is the temporal frequency, and c is the wave speed.

Therefore, outside D, the incident and scattered waves u_o, v satisfy

$$\triangle u_0(\mathbf{x}) + k^2 u_0(\mathbf{x}) = \delta(\mathbf{x}-\mathbf{x}_0) \tag{60}$$

$$\triangle v(\mathbf{x}) + k^2 v(\mathbf{x}) = 0 \tag{61}$$

and $u(\mathbf{x}) = u_0(\mathbf{x}) + v(\mathbf{x})$ is the total field, representing pressure at $\mathbf{x}$.

The mechanical and physical properties of the obstacle surface ∂D determine the boundary conditions for v

(1) Soft boundary – pressure vanishes: $u_0 + v = 0$ (Dirichlet)

(2) Hard boundary – displacement vanishes: $\frac{\partial(u_0+v)}{\partial \mathbf{n}} = 0$ (Neumann)
$\mathbf{n}$ is the outward unit normal of ∂D

We therefore have Dirichlet or Neumann boundary conditions for the scattered field v on ∂D

$$\triangle v(\mathbf{x}) + k^2 v(\mathbf{x}) = 0, \quad \mathbf{x} \in \mathbb{R}^3 \setminus \bar{D} \tag{62}$$

$$v = -u_0 \quad \text{or} \quad \frac{\partial v}{\partial \mathbf{n}} = -\frac{\partial u_0}{\partial \mathbf{n}} \quad \mathbf{x} \in \partial D \tag{63}$$

Together with the Sommerfeld radiation condition

$$\lim_{r\to\infty} r\left(\frac{\partial u}{\partial r} - iku\right) = 0 \quad r = |\mathbf{x}| \tag{64}$$

both these boundary value problems are well–posed, and uniquely determines v from the incident field u_0 on ∂D.

In the approach of the Helmholtz equation or boundary integral equation, it is always the knowledge of the incident field u_0 on the boundary ∂D that uniquely determines the scattered field. The interior D is of no concern to us, and the scattering problem is never defined inside D. We wish to explore the interior of D by re–interpreting the scattering problem in the interior.

For simplicity, we assume that the wave number k is not an interior Dirichlet or Neumann eigenvalue, and that ∂D is smooth.

Let us forget for a moment the original scattering problem by assuming that there is no obstacle in D. Then the whole space becomes free space in and outside D. Except at x_0, the incident field u_0 is well–defined everywhere, particularly in D. Under the conditions that k is not an interior Dirichlet eigenvalue, it is well–known that there exists a unique, smooth distribution α of monopole sources on ∂D whose potential matches u_0 inside D:

$$u_0(\mathbf{x}) = \int_{\partial D} G(\mathbf{x},\mathbf{y})\alpha(\mathbf{y})ds \quad \mathbf{x} \in D \tag{65}$$

where for 3–D

$$G(\mathbf{x},\mathbf{y}) = \Phi(\mathbf{x},\mathbf{y}) = \frac{1}{4\pi}\frac{e^{ik|\mathbf{x}-\mathbf{y}|}}{|\mathbf{x}-\mathbf{y}|} \tag{66}$$

We will refer to the point source at $\mathbf{x}_0$ outside D which generates the incident field u_0 as the primary source, and the monopole sources α on ∂D as the equivalent or secondary sources. To an observer in D, the primary and secondary sources look identical (or sound identical for acoustic waves).

Similarly, under the condition that k in not an interior Neumann eigenvalue, there exists a unique, smooth distribution β of dipole sources on ∂D whose potential matches u_0 inside D:

$$u_0(\mathbf{x}) = \int_{\partial D} \frac{\partial G(\mathbf{x},\mathbf{y})}{\partial \mathbf{n}(\mathbf{y})}\beta(\mathbf{y})ds, \quad \mathbf{x} \in D \tag{67}$$

The two obstacle scattering problems with Dirichlet and Neumann boundary conditions are equivalent to the determination of the equivalent (secondary) sources of monopoles or dipoles.

Theorem. Let k be not an eigenvalue and ∂D smooth. then
(i) v defined by the formula

$$v(\mathbf{x}) = -\int_{\partial D} G(\mathbf{x},\mathbf{y})\alpha(\mathbf{y})ds, \quad \mathbf{x} \in \mathbb{R}^3 \setminus D \tag{68}$$

is a solution of the Dirichlet problem
(ii) v defined by the formula

$$v(\mathbf{x}) = -\int_{\partial D} \frac{\partial G(\mathbf{x},\mathbf{y})}{\partial \mathbf{n}(\mathbf{y})}\beta(\mathbf{y})ds, \quad \mathbf{x} \in \mathbb{R}^3 \setminus D \tag{69}$$

is a solution of the Neumann problem.

Solving the obstacle scattering problem is equivalent to finding the secondary sources on ∂D. In order to find the secondary sources by interpolation, we need to define Γ, a smooth, closed curve in D, parallel and sufficiently close to ∂D. The secondary sources we seek then satisfy the equation

$$u_0(\mathbf{x}) = \int_{\partial D} G(\mathbf{x},\mathbf{y})\alpha(\mathbf{y})\, ds, \quad \mathbf{x} \in \Gamma \tag{70}$$

for the Dirichlet case and

$$u_0(\mathbf{x}) = \int_{\partial D} \frac{\partial G(\mathbf{x},\mathbf{y})}{\partial \mathbf{n}(\mathbf{y})}\beta(\mathbf{y})ds, \quad \mathbf{x} \in \Gamma \tag{71}$$

for the Neumann case.

To determine α or β, a first kind integral equation has to be solved. There are advantages and disadvantages in treating a first kind integral equation numerically. We will first discuss the advantages and then consider ways to to minimize the drawbacks. The main advantage is that the kernels are not singular – there is no need to design quadratures for singular integrals. As we have noted, even if we have available quadratures for singular integrals, it requires knowledge of the kernel $K(\mathbf{x},\mathbf{y}) = g(\mathbf{x},\mathbf{y})\, s(\mathbf{x},\mathbf{y}) + h(\mathbf{x},\mathbf{y})$, (where $s(\mathbf{x},\mathbf{y})$ is singular when $\mathbf{x} = \mathbf{y}$ and g and h are smooth) which may not be available.

In order to solve, e.g., the integral equation

$$u_0(\mathbf{x}) = \int_{\partial D} G(\mathbf{x},\mathbf{y})\alpha(\mathbf{y})\, ds, \quad \mathbf{x} \in \Gamma \tag{72}$$

it seems that we need to discretize the integral by quadrature. Instead, we may change our point of view, and there is no need to design quadrature at all – the quadrature issue can be replaced by interpolation. Why interpolation? For simplicity, we assume that the primary sources are monopoles located on Σ which is separated from ∂D by a distance d – the linear map $A : C(\Sigma) \to C(D)$ defined by the formula

$$u_0(\mathbf{x}) = (A\eta)(\mathbf{x}) =: \int_{\Sigma} G(\mathbf{x},\mathbf{y})\eta(\mathbf{y})\, ds, \quad \mathbf{x} \in D \tag{73}$$

maps the primary source η to its incident field u_0, and is a compact linear operator, with singular values decaying exponentially to zero. For a given precision ϵ, the

numerical rank of A is finite and proportional to $|\log(\epsilon)|$. This rank(A) is the number of degrees of freedom to specify, to the same precision, an arbitrary incident field u_0 in D generated by source η on Σ. Therefore, the task of finding the secondary sources on ∂D to match u_0 in D to precision ϵ becomes an issue of matching these rank(A) parameters which specify u_0 in D.

Algorithm for Obstacle Scattering by Interpolation

• **Choose** n equispaced points $\{\mathbf{y}_j\}$ on ∂D as the locations of the secondary point sources, with h as the sampling interval.

• **Choose** the parallel curve or surface Γ in D that is separated from ∂D by a constant multiple of h.

• **Place** m equispaced points $\{\mathbf{x}_i\}$ on Γ to sample u_o.

• **Solve** the m–by–n linear system with $m \geq n$

$$u_0(\mathbf{x}_i) = \sum_{j=1}^{n} G(\mathbf{x}_i, \mathbf{y}_j)\alpha_j, \quad i = 1, 2, \ldots m \tag{74}$$

for the Dirichlet case or

$$u_0(\mathbf{x}_i) = \sum_{j=1}^{n} \frac{\partial G(\mathbf{x}_i, \mathbf{y}_j)}{\partial \mathbf{n}(\mathbf{y}_j)}\beta_j, \quad i = 1, 2, \ldots m \tag{75}$$

for the Neumann case as a least–squares problem.

This is a standard least–squares problem for interpolation with basis functions $b_j(\mathbf{x}) = G(\mathbf{x}, \mathbf{y})$ and interpolation points $\mathbf{x}_i$.

The points $\{\mathbf{x}_i\}$ and $\{\mathbf{y}_j\}$ do not have to be equispaced, and there is no need for quadrature weights.

The solution $\{\alpha_j\}$ or $\{\beta_j\}$ is not an approximation to $\{\alpha(\mathbf{y}_j)\}$ or $\{\beta(\mathbf{y}_j)\}$ – it is more likely to be $\{\alpha(\, y_j)w_j\}$ or $\{\beta(\mathbf{y}_j)\, w_j\}$ where w_j are some sort of (unknown) quadrature weights.

Interpolation is not sensitive to the complication of geometry, and computer coding in two and three dimensions is simple.

The main drawback of this approach is ill-conditioning. For a fixed location of Γ, the m–by–n linear system becomes exponentially ill–conditioned as m and n increase. As a compromise, it turns out that in double precision of 16 digits, a separation of the testing locations on Γ from sources on ∂D by 3 to 4 h is ideal to balance conditioning and accuracy. h is the distance between the sources on ∂D. The numerical rank of the m–by–n linear system for a condition number of 10^8 grows linearly with n, and the scattered field v has about 8 correct digits.

9. NUMERICAL RESULTS IN $\mathbb{R}^3$ – SCATTERING OFF SOUND–SOFT AND SOUND–HARD SPHERES

As a first test of our numerical method, we will compute the scattering off sound–soft and sound–hard spheres. This is a good test, because we have an exact analytical series solution to compare against.

The exact solution [3] of an incident wave V^i created by a point source at $\mathbf{r}_0 = (r_0, 0, 0)$ such that $V^i = \frac{e^{ikR}}{kR}$ scattering off a sound soft sphere is given by :

$$V^i + V^s = i\sum_{n=0}^{\infty}(2n+1)P_n(\cos\theta)h_n^{(1)}(kr_>)[j_n(kr_<) - \frac{j_n(ka)}{h_n^{(1)}(ka)}\, h_n^{(1)}(kr_<)] \quad (76)$$

Where j_n,$h_n^{(1)}$, and P_n are spherical Bessel, spherical Hankel, and Legendre functions as defined in [1]:

$$j_n(x) \doteq \sqrt{\frac{\pi}{2x}} J_{n+\frac{1}{2}}(x) \quad (77)$$

$$h_n^{(1)}(x) \doteq \sqrt{\frac{\pi}{2x}} H_{n+\frac{1}{2}}^{(1)}(x) \quad (78)$$

and a is the radius of the sphere.

The exact solution of a point source scattering off a sound hard sphere is:

$$V^i + V^s = i\sum_{n=0}^{\infty}(2n+1)P_n(\cos\theta)h_n^{(1)}(kr_>)[j_n(kr_<) - \frac{j_n'(ka)}{h_n^{(1)'}(ka)}\, h_n^{(1)}(kr_<)] \quad (79)$$

Where the $'$ denotes the derivative:

$$j_n'(x) = -1/4\,\sqrt{2}J_{n+\frac{1}{2}}(x)\pi\frac{1}{\sqrt{\frac{\pi}{x}}}x^{-2} + 1/2\,\sqrt{2}\sqrt{\frac{\pi}{x}} \left(-J_{n+\frac{3}{2}}(x) + \frac{(n+1/2)\,J_{n+\frac{1}{2}}(x)}{x}\right) \quad (80)$$

$$h_n^{(1)'}(x) = -1/4\,\sqrt{2}H_{n+\frac{1}{2}}^{(1)}(x)\pi\frac{1}{\sqrt{\frac{\pi}{x}}}x^{-2} + 1/2\,\sqrt{2}\sqrt{\frac{\pi}{x}} \left(-H_{n+\frac{3}{2}}^{(1)}(x) + \frac{(n+1/2)\,H_{n+\frac{1}{2}}^{(1)}(x)}{x}\right) \quad (81)$$

These equations were computed in Matlab to machine precision (10^{-16}).

Our scattering surface ∂D is a sphere of radius 1 centered at the origin $(0, 0, 0)$. In order to implement our interpolation method, we need to place n equispaced points $\{\mathbf{y}_j\}$ on ∂D as locations of the secondary sources, and m points $\{\mathbf{x}_i\}$ on the surface of the the smaller sphere Γ inside D of radius r_Γ as the testing locations. In order to do so, we create an algorithm that places points spaced approximately h apart in both longitude and latitude. This quasi-uniform spacing was used for both

the location of the secondary sources $\{\mathbf{y}_j\}$ on ∂D and the location of the sampling points $\{\mathbf{x}_i\}$ on the sphere Γ, also located at the origin, but with a radius $1 - 3\,h$.

The interpolation algorithm was coded in ANSI C. The results in Table 1–2 and Figure 2 were obtained on a Pentium II 266MHz PC running Linux and compiled using GCC[3], while the results in Figure 3 were obtained on an Sun Ultra–80 workstation using the Sun C compiler. In both cases the LAPACK[2] complex SVD based least–squares routine ZGELSS was used to solve the linear system. Under Linux, good performance was obtained by utilizing the BLAS from the ATLAS project [4]. Matlab [5] was used to compute the analytic series solution, as well as for visualization.

Table 1 shows numerical convergence results for $k = 5$. The point source is located at $(2, 0, 0)$, and the measurement locations are at $(5, 0, 0)$ (the backscattered wave) and $(-5, 0, 0)$ (the shadow region). The total field $V^i + V^s$ is shown. `r_g` is r_Γ, the radius of the inner surface Γ. `sec` represents the wall clock running time of the code, rounded to the nearest second. The last line of the table shows the result of equations (76) and (79).

Table 1.

Point source at (2,0,0) scattering off a sound-soft sphere at (0,0,0) of radius a=1, ka = 5

m	n	~h	r_g	(5,0,0) real	(5,0,0) imag	(-5,0,0) real	(-5,0,0) imag	cond(A)	sec
87	57	0.4	0.4	-6.7142802627e-02	4.4483587304e-02	6.4686330664e-03	-8.1311232739e-04	4.5e+03	<1
142	128	0.3	0.4	-6.6453078943e-02	4.4201263537e-02	6.2069894822e-03	-1.4773976973e-03	2.5e+05	<1
359	273	0.2	0.4	-6.6451940499e-02	4.4198987138e-02	6.2071128956e-03	-1.4764840918e-03	1.5e+08	8
	analytic			-6.6451940370e-02	4.4198987320e-02	6.2071127911e-03	-1.4764844458e-03		

Point source at (2,0,0) scattering off a sound-hard sphere at (0,0,0) of radius a=1, ka = 5

m	n	~h	r_g	(5,0,0) real	(5,0,0) imag	(-5,0,0) real	(-5,0,0) imag	cond(A)	sec
87	57	0.4	0.4	-3.6383633845e-02	3.8638506818e-02	2.0634359690e-02	-2.8529687181e-02	3.1e+03	<1
142	128	0.3	0.4	-3.7652381946e-02	3.7828789148e-02	2.0309935926e-02	-2.8089469539e-02	1.1e+05	<1
359	273	0.2	0.4	-3.7653861003e-02	3.7832489048e-02	2.0304918393e-02	-2.8093988607e-02	4.2e+07	9
	analytic			-3.7653862030e-02	3.7832486880e-02	2.0304919427e-02	-2.8093984709e-02		

Table 2 shows the convergence results for $k = 10$. Note the high order convergence is clearly visible – as n is approximately doubled from 273 to 523 the number of correct digits approximately doubles. Figure 2 shows a plot of $0^0 \to 180^0$ at radius 5, with the lower plot showing the residuals between the numerical method and and the analytical series solution (although the magnitude of the complex total field is plotted), different from the real and imaginary results presented in Table 1).

[3] `http://www.gnu.org`
[4] `http://www.netlib.org/atlas`
[5] `http://www.mathworks.com`

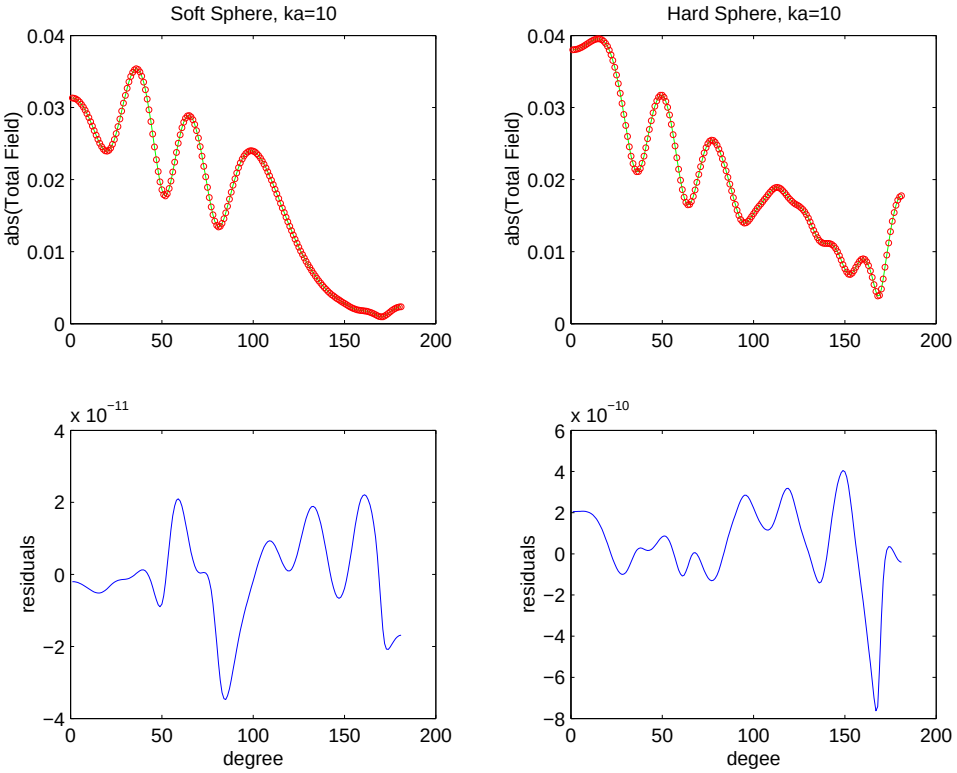

FIG. 2. Numerical results of a point source scattering off a sphere, $ka = 10$

Table 2.

Point source at (2,0,0) scattering off sound-soft sphere at (0,0,0) of radius a=1, ka = 10

m	n	~h	r_g	(5,0,0) real	(5,0,0) imag	(-5,0,0) real	(-5,0,0) imag	cond(A)	sec
87	57	0.4	0.4	-1.1891195081e-03	-3.5159612472e-02	-9.2353883066e-03	7.1579561525e-04	1.6e+02	<1
142	128	0.3	0.4	1.0929161580e-03	-3.0797604413e-02	4.3815531014e-03	-2.8674773093e-03	2.6e+04	<1
359	273	0.2	0.4	-2.4256150170e-03	-3.1248300099e-02	1.4789099386e-03	-1.8234637170e-03	3.4e+07	8
612	523	0.15	0.5	-2.4306505313e-03	-3.1234187810e-02	1.4827205481e-03	-1.8190039826e-03	1.5e+07	51
1361	1186	0.1	0.7	-2.4306503392e-03	-3.1234187450e-02	1.4827172492e-03	-1.8190039395e-03	1.1e+07	585
analytic				-2.4306503468e-03	-3.1234187447e-02	1.4827172421e-03	-1.8190039235e-03		

Point source at (2,0,0) scattering off sound-hard sphere at (0,0,0) of radius a=1, ka = 10

m	n	~h	r_g	(5,0,0) real	(5,0,0) imag	(-5,0,0) real	(-5,0,0) imag	cond(A)	sec
87	57	0.4	0.4	9.8448546678e-03	-3.3325141244e-02	-8.6282279899e-03	5.1160218371e-04	2.5e+02	<1
142	128	0.3	0.4	1.1557475756e-02	-4.0235301753e-02	-7.1020835532e-03	-1.7694079884e-02	3.9e+02	<1
359	273	0.2	0.4	1.2085769118e-02	-3.6015814670e-02	-3.3066103015e-03	-1.7431523327e-02	2.1e+07	8
612	523	0.15	0.55	1.2114295862e-02	-3.6031960744e-02	-3.3107428813e-03	-1.7435787053e-02	5.5e+06	52
1361	1186	0.1	0.7	1.2114294325e-02	-3.6031963236e-02	-3.3106965141e-03	-1.7435790404e-02	2.3e+06	607
analytic				1.2114294460e-02	-3.6031963407e-02	-3.3106960214e-03	-1.7435790456e-02		

Figure 3 shows the results for $k = 25$. In this figure, $n = 10015$, $m = 12234$, $h = 0.035$, and $r_\Gamma = 0.8775$. This large matrix A (1.8e+09 bytes of main memory) took about 100 hours to solve on a Sun Ultra80 (440Mhz), although the machine was heavily loaded so the timing is not precise. The condition number of the the

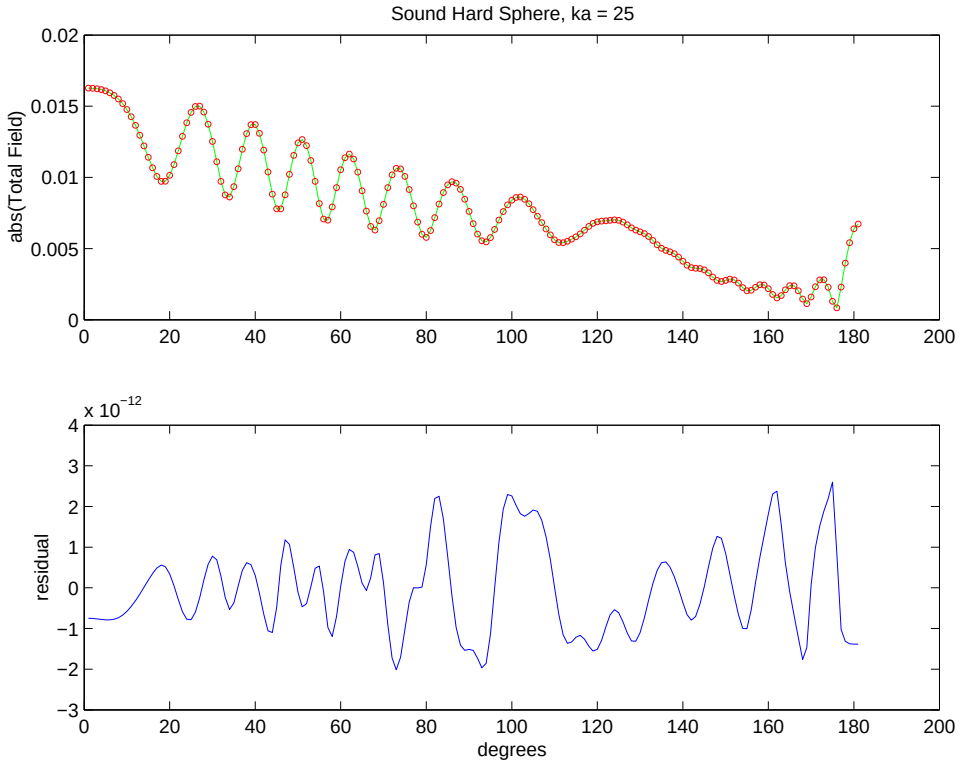

FIG. 3. Numerical results of a point source scattering off a hard sphere, $ka = 25$

matrix A was 9.2e+06. Note again the high accuracy of the results compared to the analytical series solution. Obviously, direct methods for high frequencies scattering in $\mathbb{R}^3$ are not practical. It is possible to increase the efficiency of boundary integral formulations of scattering by using the Fast Multipole Method [9], although the coding complexity increases by orders of magnitude.

10. AXISYMMETRIC SCATTERING BY INTERPOLATION

In this section we describe axisymmetric reduction of the problem, and the corresponding drastic reduction in computational requirements.

We describe our scattering surface–of–rotation ∂D as a simple smooth curve in $\mathbb{R}^2$ represented by the trigonometric interpolating polynomials $x(t)$ and $y(t)$ rotated around the $\hat{x}$ axis

$$\partial D: \quad \mathbf{y}(t,\theta) = x(t)\,\hat{x} + y(t)\,\cos\theta\,\hat{y} + y(t)\,\sin\theta\,\hat{z} \tag{82}$$

We require $y(t) > 0$ so that our surface–of–rotation remains doubly connected. Similarly, we define the testing surface–of–rotation Γ inside ∂D by rotating trigonometric interpolating polynomials $x_\Gamma(\tau)$ and $y_\Gamma(\tau)$ around the $\hat{x}$ axis

$$\Gamma: \quad \mathbf{x}(\tau,\phi) = x_\Gamma(\tau)\,\hat{x} + y_\Gamma(\tau)\,\cos\phi\,\hat{y} + y_\Gamma(\tau)\,\sin\phi\,\hat{z} \tag{83}$$

It is convenient to define a complex function $w(t)$ and the Fourier series

$$w(t) = \sum A_m \, e^{i\,m\,t} \tag{84}$$

with Fourier coefficients A_m so that $x(t)$ is the real component of $w(t)$ and $y(t)$ is the imaginary component of $w(t)$: $w(t) = x(t) + i\,y(t)$. Similarly, we define the complex function $w_\Gamma(t)$ and the Fourier series

$$w_\Gamma(\tau) = \sum B_m \, e^{i\,m\,\tau} \tag{85}$$

and the Fourier coefficients B_m to represent $x_\Gamma(\tau)$ and $y_\Gamma(\tau)$: $w_\Gamma(\tau) = x_\Gamma(\tau) + i\,y_\Gamma(\tau)$.

The distance between the sources $\{\mathbf{y}_j\}$ on the surface ∂D and the points $\{\mathbf{x}_i\}$ on the sampling surface Γ is

$$\begin{aligned} &R(\mathbf{x},\mathbf{y}) = |\mathbf{x}-\mathbf{y}| \\ &= \sqrt{(x(t)-x_\Gamma(\tau))^2 + (y(t)\cos\theta - y_\Gamma(\tau)\cos\phi)^2 + (y(t)\sin\theta - y_\Gamma(\tau)\sin\phi)^2} \end{aligned} \tag{86}$$

If we allow only axisymmetric incident waves (i.e. in our case point sources located on the $\hat{x}$ axis), then we can set $\phi = 0$, and sample the sum of our axisymmetric Greens functions (dipole ring sources) only at $\mathbf{x}_i = x_\Gamma(\tau_i)\,\hat{x} + y_\Gamma(\tau_i)\,\hat{y}$. We then get the interpolation method for axisymmetric exterior sound–hard scattering

$$u_0(\mathbf{x}_i) = \sum_{j=1}^{n} \frac{\partial G(\mathbf{x}_i,\mathbf{y}_j)}{\partial \mathbf{n}(\mathbf{y}_j)} \beta_j, \quad i = 1, 2, \ldots m \tag{87}$$

$$u_0(\mathbf{x}_i) = \sum_{j=1}^{n} \left[\int_0^{2\pi} \nabla \frac{e^{ikR(\mathbf{x}_i,\mathbf{y}_j)}}{R(\mathbf{x}_i,\mathbf{y}_j)} \cdot \mathbf{n}(\mathbf{y}_j)\, d\theta \right] \beta_j, \quad i = 1, 2, \ldots m \tag{88}$$

where

$$\begin{aligned} &\nabla \frac{e^{ikR(\mathbf{x}_i,\mathbf{y}_j)}}{R(\mathbf{x}_i,\mathbf{y}_j)} \cdot \mathbf{n}(\mathbf{y}_j) = \\ &\left[\frac{i\,k e^{ikR}}{R^2} - \frac{e^{ikR}}{R^3} \right] [x(t_j) - x_\Gamma(\tau_i)]\, n_x(t_j) + [y(t_j)\, n_y(t_j)] - [y_\Gamma(\tau_i)\, n_y(t_j)\, \cos\theta] \end{aligned} \tag{89}$$

where $n_x(t_j)$ is the $\hat{x}$ component of unit normal $\mathbf{n}(\mathbf{y}_j)$ at point $\mathbf{y}_j$ on ∂D, and $n_y(t_j)$ is the $\hat{y}$ component of unit normal $\mathbf{n}(\mathbf{y}_j)$ at point $\mathbf{y}_j$ on ∂D. Because in our interpolation method the surface ∂D with the secondary dipole ring sources $\{\mathbf{y}_j\}$ is separated by a constant multiple from the points $\{\mathbf{x}_i\}$ on Γ where we sample u_0, the integral

$$\int_0^{2\pi} \nabla \frac{e^{ikR(\mathbf{x}_i,\mathbf{y}_j)}}{R(\mathbf{x}_i,\mathbf{y}_j)} \cdot \mathbf{n}(\mathbf{y}_j)\, d\theta \tag{90}$$

is never singular, and so we can use a (simple) trapezoidal rule quadrature method (equation (29)) to calculate the entries to the m–by–n matrix A.

A similar method can of course be easily developed for sound–soft scattering, but this method was not implemented, as we are primarily interested in sound–hard scattering problems.

11. NUMERICAL RESULTS OF AXISYMMETRIC SCATTERING BY INTERPOLATION

The previous section verified that the interpolation method provides for high–order convergence for the scattering off spheres in $\mathbb{R}^3$. We then used this verified code to solve the axisymmetric scattering problem of a torus (donut). For this test, we put points over the entire surface of the torus in $\mathbb{R}^3$, in order to have a result with which to compare the axisymmetric reduction.

We define the torus as a surface of revolution around the $\hat{x}$ axis. Figure 4 shows the 2–D plot of a circle of radius 1 centered at $(3, 3, 0)$. If this circle is rotated around the $\hat{x}$ axis, the torus surface ∂D shown in green in figure 1 is created. (The red sphere in figure 1 shows the location of the point source creating the incident field u_0). We place n secondary dipole ring sources $\{\mathbf{y}_j\}$ on ∂D and m sampling locations $\{\mathbf{x}_i\}$ on the surface Γ, which is a torus of smaller minor radius r_Γ inside the torus ∂D:

$$\mathbf{y}(t,\theta) = (3+\cos t)\,\hat{x} + ((3+\sin t)\,\cos\theta)\,\hat{y} + ((3+\sin t)\,\sin\theta)\,\hat{z} \tag{91}$$

$$\mathbf{x}(\tau,\phi) = (3+r_\Gamma\,\cos\tau)\,\hat{x} + ((3+r_\Gamma\,\sin\tau)\,\cos\phi)\,\hat{y} + ((3+r_\Gamma\,\sin\tau)\,\sin\phi)\,\hat{z} \tag{92}$$

Table 3 shows the convergence results for the $\mathbb{R}^3$ algorithm for an increasing number of points (and a correspondingly smaller h). The two measurement locations were $(10, 0)$ and $(-10, 0)$. Note that we get about 5-6 correct digits.

Table. 3.

Point Source Scattering off a Torus

Hard Scattering off a Donut: circle centered at (3,3) with radius 1 rotated around x axis

k = 1 Points in R^3

m	n	~h	r_g	(10,0) real	(10,0) imag	(-10,0) real	(-10,0) imag	cond	sec
251	210	0.7	0.3	-6.8402134678e-02	2.3976207623e-02	-1.1301001068e-01	6.2222169092e-03	6.7e+03	2
374	310	0.6	0.3	-8.4305463283e-02	-1.0179648780e-02	-1.3346522589e-01	1.6212337206e-02	6.1e+04	7
525	445	0.5	0.3	-8.9229986033e-02	-7.1128473763e-03	-1.3533949940e-01	1.5831504544e-02	2.9e+05	22
845	699	0.4	0.3	-8.9828706466e-02	-8.5026669554e-03	-1.3242508076e-01	1.5506175021e-02	5.3e+06	109
1501	1244	0.3	0.3	-8.8124939118e-02	-8.1715076674e-03	-1.3086030255e-01	1.6607440079e-02	2.5e+09	570
3630	2906	0.2	0.4	-8.7948648088e-02	-8.3274404979e-03	-1.3078400506e-01	1.6689566175e-02	3.2e+10	6994
6392	5135	0.15	0.55	-8.7948638110e-02	-8.3274279587e-03	-1.3078399705e-01	1.6689568333e-02	1.6e+11	52513
				Axisymmetric Reduction					
37	31	0.2	0.4	-8.7948638112e-02	-8.3274279611e-03	-1.3078399705e-01	1.6689568334e-02	2.9e+06	<1

The last line in table 3 (labeled "Axisymmetric Reduction") shows the results of implementing equation (87). The red circles in figure 4 show the location of the n secondary dipole ring sources $\{\mathbf{y}_j\}$, and the green circles show the location of the m sampling locations $\{\mathbf{x}_i\}$ on Γ. The black circle shows the location of the point source creating the incident field u_0. The entire scattering algorithm was implemented in 81 lines of matlab code. After verifying the results versus the full $\mathbb{R}^3$ version, the algorithm was reimplemented in ANSI C (and as before, using

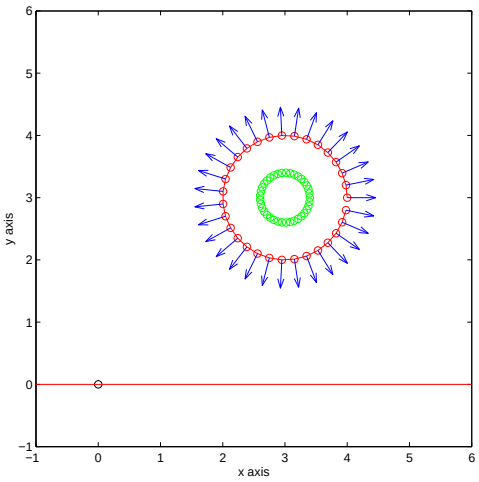

FIG. 4. This figure shows the location of the points for axisymmetric reduction for a point source (black circle) scattering off the torus defined by rotating the red circle around the $\hat{x}$ axis

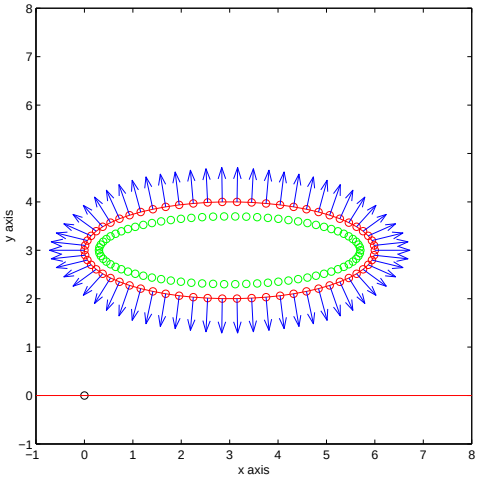

FIG. 5. This figures shows the location of the points for axisymmetric reduction for a point source (black circle) scattering off the elliptical torus (squashed donut) defined by rotating the red ellipse around the $\hat{x}$ axis

LAPACK and ATLAS BLAS for the SVD). The axisymmetric reduction and C code reduced the solve time from a couple days to less than a second. In the C code, an adaptive trapezoidal rule quadrature algorithm was used to compute the integral in the dipole ring source term, and we check for at least 10 digits of accuracy.

Tables 4–5 show convergence results for $k = 5$ and $k = 10$.

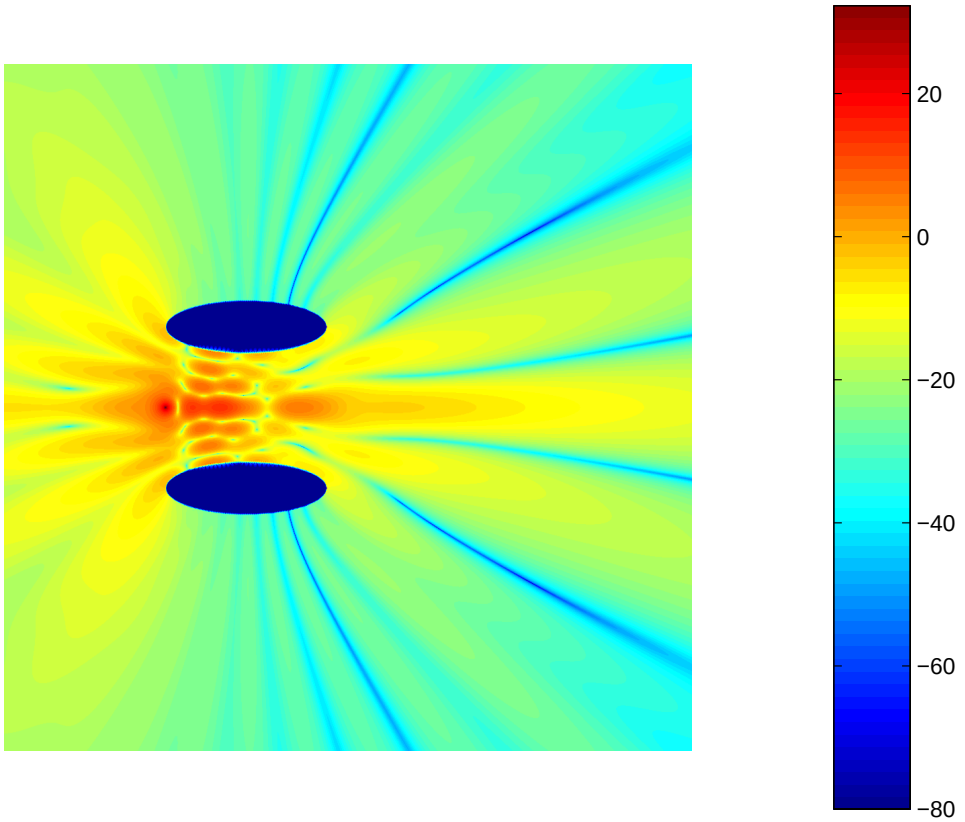

FIG. 6. A visualization of the total field from a point source scattering through the elliptical torus waveguide defined in figure 5. The dimensions are 12 by 12. k = 5. The colormap represents the pressure field in Decibels..

Table 4. Axisymmetric Sound Hard Torus Scattering Convergence Results

k = 5,

m	n	~h	r_g	(10,0) real	(10,0) imag	(-10,0) real	(-10,0) imag	cond	sec
37	31	0.2	0.5	-1.5050898714e-02	1.1303110197e-02	-5.3347553214e-02	1.0483839016e-01	7.3e+04	<1
74	62	0.1	0.7	-1.5050872665e-02	1.1303107622e-02	-5.3347555121e-02	1.0483839201e-01	1.3e+05	<1
150	125	0.05	0.85	-1.5050872670e-02	1.1303107633e-02	-5.3347555111e-02	1.0483839203e-01	6.8e+04	<1

k = 10,

m	n	~h	r_g	(10,0) real	(10,0) imag	(-10,0) real	(-10,0) imag	cond	sec
37	31	0.2	0.5	1.8034877708e-01	3.2296444198e-02	2.3977385065e-01	-4.0453620709e-01	3.4e+04	<1
74	62	0.1	0.7	1.8039297194e-01	3.2218774642e-02	2.3981373926e-01	-4.0446175188e-01	1.2e+05	<1
150	125	0.05	0.85	1.8039297332e-01	3.2218774621e-02	2.3981373907e-01	-4.0446175185e-01	7.4e+04	<1

Note the high–order convergence.

Figure 5 shows an ellipse that defines a “squashed donut” waveguide. Table 5 shows the convergence results. Figure 6 shows a visualization of the total field at 1024 x 768 field points. The log mag of the total field is colormapped in dB using the default Matlab colormap. This high resolution image took about 24 hours

to produce on heavily loaded Sun Ultra 80 workstation. We suspect that with a less–loaded workstation, cache reuse would improve this time considerably.

Table 5.

Axisymmetric Sound Hard Elliptical Torus (squashed donut) Convergence Results

k=5

m	n	~h	r_g	(10,0) real	(10,0) imag	(-10,0) real	(-10,0) imag	cond	sec
74	62	0.1	0.7	-5.3571562584e-01	-2.1116739591e-01	2.8317361784e-01	3.0781477949e-01	2.9e+04	<1
150	125	0.05	0.85	-5.3423678507e-01	-2.1071284520e-01	2.8344284218e-01	3.0785039808e-01	3.4e+04	<1
301	251	0.025	0.925	-5.3421376870e-01	-2.1066971152e-01	2.8339399888e-01	3.0780424972e-01	2.1e+04	4

12. CONCLUSION

We have presented a simple, high–order method for the numerical solution of sound propagating through sound–hard waveguides. A future research goal is to use this algorithm as the forward component in solving an inverse problem. In the design of modern high–power loudspeakers, directional horns are used to increase the efficiency of radiated sound [6]. When loudspeakers with horns are used together to provide sound for large auditoriums, it is important to use horns with the correct coverage pattern, so each section of seats is covered by only one loudspeaker. By specifying the desired coverage pattern and solving an inverse scattering problem [7], it should be possible to optimize loudspeaker horn geometry to improve the coverage patterns and acoustic characteristics of modern high–power loudspeakers.

[6] see `http://www.meyersound.com` for information on high–power horn loudspeakers, especially the paper about the design of the horn loudspeaker system that was recently installed in Carnegie Hall, New York. A good reference is from Harry Olson [21], who was the director RCA labs, where most of this technology was invented in the 1930's and 1940's.

REFERENCES

1. Milton Abramowitz and Irene A. Stegun, editors. *Handbook of Mathematical Functions With Formulas, Graphs, and Mathematical Tables*. Dover, New York, N.Y., 1972.
2. E. Anderson, Z. Bai, C. Bischof, S. Blackford, J. Demmel, J. Dongarra, J. Du Croz, A. Greenbaum, S. Hammarling, A. McKenney, and D. Sorensen, editors. *LAPACK Users Guide (Third Edition)*. Society for Industrial and Applied Mathematics (SIAM), Philedelphia, PA, 2000. `http://www.netlib.org/lapack`.
3. J. J. Bowman, T.B.A Senior, and P.L.E. Uslenghi, editors. *Electromagnetic and Acoustic Scattering by Simple Shapes*. North Holland, Amsterdam, 1969.
4. Oscar P. Bruno and Leonid A. Kunyansky. Fast, high-order solution of surface scattering problems. In Alfredo Bermudez et al., editor, *Fith International Conference on Mathematical and Numerial Aspects of Wave Propagation*, pages 465–470. Society for Industrial and Applied Mathematics, 2000.
5. Lawrence F. Canino, John J. Ottusch, Mark A. Stalzer, John L. Visher, and Stephan M. Wandzura. Numerical solution of the Helmholtz equation in 2d and 3d using a high–order Nystrom discretization. *Journal of Computational Physics*, 146:627–663, 1998.
6. YH Chen, WC Chew, and S Zeroug. Fast multipole method as an efficient solver for 2d elastic wave surface integral equations. *Computational Mechanics*, 20(6):485–506, 1997.
7. Yu Chen. Inverse scattering via Heisenberg's uncertainty principle. *Inverse Problems*, 13(2):253–282, 1997.
8. Yu Chen and Sang-Yeun Shim. Solution of obstacle scattering problems by interpolation. Presented 9 October 2000 at The Courant Institute Numerical Analysis Seminar, (manuscript in preparation).
9. H Cheng, L. Greengard, and V. Rokhlin. A fast adaptive multipole algorithm in three dimensions. *Journal of Computational Physics*, 155:468–498, 1999.
10. David Colton and Rainer Kress. *Inverse Acoustic and Electromagnetic Scattering Theory, Second Edition*. Springer–Verlag, Berlin, 1998.
11. Adrian Doicu, Yuri Eremin, and Thomas Wriedt. *Acoustic and Electromagnetic Scattering Analysis Using Discrete Sources*. Academic Press, San Diego, CA, 2000.
12. I.S. Gradshteyn, I.M Ryzhik, and Alan Jeffrey, editors. *Table of Integrals, Series, and Products*. Academic Press, San Deigo, CA., fifth edition, 1994.
13. James J. Grannell, Joseph J. Shirron, and Luise S. Couchman. A hierarchic p-version boundary–element method for axisymmetric acoustic scattering and radiation. *Journal of the Acoustical Society of America*, 95(5):2320–2329, 1994.
14. JS Jhao and WC Chew. Three-dimensional multilevel fast multipole algorithm from static to electrodynamic. *MICROW OPT TECHN LET*, 26(1):43–48, 2000.
15. Rainer Kress. On constant alpha force–free fields. *Journal of Engineering Math*, 20:323–344, 1986.
16. Rainer Kress. On the numerical solution of a hypersingular integral equation in scattering theory. *Journal of Computational and Applied Mathematics*, 61:345–360, 1995.
17. N.N. Lebedev. *Special Functions and Their Applications*. Dover, New York, 1972.
18. Gregory Matviyenko. On the azimuthal Fourier components of the Green's function for the Helmholtz equation in three dimensions. *Journal of Mathematical Physics*, 36(9):5159–5169, 1995.
19. Philip M. Morse and K. Uno Ingard. *Theoretical Acoustics*. Princeton University, Princeton, NJ, 1986.
20. Ramesh Natarajan. An iterative scheme for dense, complex-symetric, linear systems in acoustics boundary-element computations. *SIAM Journal on Scientific Computing*, 19(5):1450–1470, 1998.
21. Harry F. Olson. *Acoustical Engineering*. D. Van Nostrand Company, Princeton, N.J., 1957.
22. JM Song, CC Lu, and WC Chew. Fast Illinois solver code (FISC). *IEEE ANTENNAS PROPAG*, 40(3):27–35, 1998.
23. W. W. Symes. Cell–centered finite difference modeling for the 3-d Helmholtz problem. Technical report, Rice University, 1996.
24. W. W. Symes. Iterative procedures for wave propagation in the frequency domain. Technical report, Rice University, 1996.